

Multiple Kinetic Intermediates Accumulate during the Unfolding of Horse Cytochrome *c* in the Oxidized State[†]

Abani K. Bhuyan and Jayant B. Udgaonkar*

National Centre for Biological Sciences, TIFR Centre, P.O. Box 1234, Indian Institute of Science Campus, Bangalore 560012, India

Received March 2, 1998; Revised Manuscript Received April 8, 1998

ABSTRACT: The unfolding kinetics of horse cytochrome *c* in the oxidized state has been studied at 10, 22, and 34 °C as a function of guanidine hydrochloride (GdnHCl) concentration. Rapid (millisecond) measurements of far-UV circular dichroism (CD) as well as fluorescence quenching due to tryptophan to heme excitation energy transfer have been used to monitor the unfolding process. At 10 °C, the decrease in far-UV CD signal that accompanies unfolding occurs in two phases. The unobservable burst phase is complete within 4 ms, while the slower phase occurs over tens to hundreds of milliseconds. The burst phase unfolding amplitude increases cooperatively with an increase in GdnHCl concentration, exhibiting a transition midpoint of 3.2 M at 10 °C. In contrast, no burst phase change in fluorescence occurs during unfolding at 10 °C. At 22 and 34 °C, both the fluorescence-monitored unfolding kinetics and the far-UV CD-monitored unfolding kinetics are biphasic. At both temperatures, the two probes yield burst phase unfolding transitions that are noncoincident with respect to the transition midpoints as well as the dependency of the burst phase amplitudes on GdnHCl concentration. The results suggest that at least two kinetic unfolding intermediates accumulate during unfolding. One burst phase intermediate, I_U^1 , has lost virtually all the native-state secondary structure, while the other burst phase intermediate, I_U^2 , has lost both secondary structure and native-like compactness. The presence of kinetic unfolding intermediates is also indicated by the nonlinear dependence of the logarithm of the apparent unfolding rate constant on GdnHCl concentration, which is particularly pronounced at 10 and 22 °C. Analysis of the burst phase unfolding transitions obtained using the two probes shows that the stabilities of I_U^1 and I_U^2 decrease steadily with an increase in temperature from 10 to 34 °C, suggesting that the structures present in them are stabilized principally by hydrogen bonding interactions.

Recent reports demonstrating the accumulation of kinetic intermediates during the unfolding of a few proteins, namely, ribonuclease A (1, 2), *E. coli* dihydrofolate reductase (3), and barstar (4, 5) have raised some new questions. How fast and how do proteins unfold? Are kinetic unfolding intermediates productive for unfolding? Is the unfolding reaction an exact reversal of the folding process? What is the nature of energy barrier(s) for unfolding? How could the knowledge of unfolding intermediates provide insight into the conformational search problem? In the endeavor of understanding these issues, detailed kinetic investigation of protein unfolding has become inevitable.

Here we report the detection of two kinetic intermediates during the unfolding of horse cytochrome *c* in the oxidized state (cyt *c* or ferricyt *c*), when probed by far-UV circular dichroism (CD) and quenching of tryptophan fluorescence. A slight curvature in the plot of the logarithm of apparent unfolding rate constants vs denaturant concentration was observed in the first report of kinetic measurements of

unfolding of oxidized horse cyt *c* by Tanford and colleagues (6). Although different degrees of curvature in the plot of log rate vs denaturant concentration have also been observed in recent unfolding studies of ferricyt *c* (7–10), the origin of the nonlinear dependence of unfolding rates on denaturant concentration has remained unknown.

Suspecting the involvement of kinetic unfolding intermediate(s) in giving rise to the curvature, we have quantitated accurately the signal amplitudes during unfolding of cyt *c* as a function of GdnHCl concentration. The unfolding kinetics measured by far-UV CD as well as tryptophan fluorescence at 10, 22, and 34 °C suggest that at least two structurally distinct kinetic intermediates accumulate very rapidly during unfolding. One intermediate (I_U^1) is shown to be devoid of nearly all the secondary structure characteristic of the fully folded protein, while the other (I_U^2) has lost both secondary structure and native-like compactness.

MATERIALS AND METHODS

Commercially available horse cyt *c* (Type VI from Sigma) was used without further purification. Concentrations of GdnHCl (Gibco BRL) in solutions were determined by refractive index measurement (11) using an Abbe-type refractometer (Milton Roy). All experiments were done in 0.1 M sodium phosphate buffer, pH 7.0. During optical

[†] This work was funded by the Tata Institute of Fundamental Research and the Department of Science and Technology, Government of India. J.B.U. is the recipient of a Golden Jubilee Biotechnology Fellowship from the Government of India.

* Author to whom correspondence should be addressed. Fax: 91-80-3343851. E-mail: jayant@ncbs.tifrbng.res.in.

measurements at 10 °C, a constant stream of nitrogen was blown on the outer surface of cuvettes and flow cells to avoid vapor condensation.

Measurement and Analysis of Equilibrium Unfolding Data. Cyt *c* solutions (5.5 and 12 μM protein for fluorescence and far-UV CD measurements, respectively) containing different concentrations of GdnHCl were incubated at the required temperature for ~2 h. Tryptophan fluorescence excited at 280 nm (slit width 0.5 nm) was measured at 358 nm (slit width 1.25 nm) in a photon counting instrument (SPEX 320). Far-UV ellipticity at 222 nm was measured using a JASCO J720 spectropolarimeter.

The fluorescence data after correcting for denaturant-dependent buffer signals were normalized by dividing by the fluorescence signal of the unfolded protein in the presence of the highest concentration of GdnHCl used. The equilibrium CD data were normalized in a similar manner by using the ellipticity value of the native protein in the presence of 0.15 M GdnHCl. To obtain the total expected signal (unfolded minus folded) in a given GdnHCl concentration, the pre- and post-transition baselines were linearly extrapolated to abscissa values of 6 and 0 M, respectively. The normalized data were least-squares fitted to a two-state N \rightleftharpoons D model according to (12, 13)

$$S_{\text{obs}} = \frac{S_f + m_f[D] + S_u + m_u[D] \exp\left(\frac{-\Delta G + m_G[D]}{RT}\right)}{1 + \exp\left(\frac{-\Delta G + m_G[D]}{RT}\right)} \quad (1)$$

where S_{obs} is the observed signal, S_f and S_u and m_f and m_u represent intercepts and slopes of native and unfolded baselines, respectively, m_G is a parameter related to exposure of hydrophobic groups upon global unfolding of the protein, and $[D]$ represents the concentration of GdnHCl. The baselines are assumed to be dependent linearly on GdnHCl concentration.

Measurement and Analysis of Unfolding Kinetics. A three-syringe mixing module (Biologic SFM-3) regulated at the required temperature by the use of an external water bath was used for kinetic measurements. The fluorescence excitation source (280 nm) was a 150 W xenon lamp. Fluorescence of the mixed solution, contained in a 1.5 mm square flow cell, was measured using a 320-nm band-pass filter. About 10 traces were averaged. Kinetic CD data at 222 nm were acquired by interfacing the SFM3 module with the JASCO J720 unit. Typically, 20 traces were averaged to reduce the noise.

Unfolding was initiated by diluting a 325 μM solution of cyt *c* in folding buffer (0.1 M sodium phosphate buffer, pH 7.0) into unfolding conditions. Folded protein solution (33 μL) was mixed with 267 μL of unfolding buffer containing a variable concentration of GdnHCl. Thus, the final protein concentration was ~32 μM. The waste solutions from the flow cell were collected to check the final concentration of GdnHCl in the reaction medium.

The averaged data points were fitted to single-exponential functions to obtain the apparent unfolding rate, λ , the initial signal, A_0 , which corresponds to the zero time or burst phase signal in the stopped-flow time window, and the final equilibrium signal, A_∞ . After subtracting the buffer signals,

the A_0 and A_∞ values were normalized with respect to the fluorescence signal of the unfolded protein or the ellipticity value of the native protein, and fitted to eq 1.

RESULTS

Figure 1 presents a few representative kinetic traces showing the time dependences of fluorescence and far-UV CD signals that have been used to monitor the unfolding of cyt *c* in different concentrations of GdnHCl at 10 and 22 °C. In Figure 1a, it is seen that the decrease in far-UV ellipticity that accompanies unfolding at 10 °C occurs in two phases. One kinetic phase, the burst phase, is over within 4 ms and is therefore not observable in the stopped-flow window. The second kinetic phase of unfolding occurs over hundreds of milliseconds. The amplitude of the burst phase is seen to be substantial, even at the lowest concentration of GdnHCl shown, and increases cooperatively with increasing concentrations of GdnHCl used to unfold the protein. In contrast, the increase in fluorescence that accompanies unfolding at 10 °C (Figure 1c) appears to occur in a single kinetic phase for each of the two lower concentrations of GdnHCl shown: extrapolation of the two kinetic unfolding curves to $t = 0$ yields values of fluorescence, A_0 , which are identical to the value expected of the fluorescence of fully folded protein.

At 22 °C (Figure 1b,d) or at 34 °C (data not shown), the unfolding kinetics are, however, biphasic when monitored by either fluorescence or far-UV CD. For all concentrations of GdnHCl shown in Figure 1b,d, large burst phase changes in both ellipticity and fluorescence can be seen.

Unfolding Kinetics at 10 °C. In Figure 2a,b, the values of A_0 and A_∞ , obtained from the values of the kinetic unfolding curves extrapolated to $t = 0$ and at $t = \infty$, respectively, are shown relative to the values of the corresponding signals obtained for the equilibrium unfolded protein. For each set of measurements, the A_∞ values reproduce the respective equilibrium unfolding signals closely, indicating that the unfolding kinetics was recorded for long enough for the protein to reach equilibrium. In Figure 2a, it is seen that the ellipticity-monitored A_0 values do not fall on the baseline of the unfolded protein constructed by extrapolating the folded protein baseline into unfolding regions. The amplitude of the burst phase decrease in ellipticity accompanying unfolding increases cooperatively with GdnHCl concentration. For concentrations of GdnHCl larger than 4 M, virtually the entire decrease in ellipticity occurs in the burst phase of unfolding. In comparison, it is seen in Figure 2b that the fluorescence-monitored A_0 values fall on the extrapolated folded protein baseline, except for GdnHCl concentrations larger than 5.0 M.

The equilibrium unfolding transitions in Figure 2a,b as well as the dependence of A_0 on GdnHCl concentration (the burst phase unfolding transition) in Figure 2a were fit to two-state unfolding transitions, using eq 1. The values for the thermodynamic parameters obtained are listed in the legend to Figure 2. Far-UV CD and fluorescence-monitored unfolding transitions yield, as expected, values for these parameters for equilibrium unfolding that are the same within experimental error.

In Figure 2c, the apparent rate constants for the single observable phase of unfolding of ferricyt *c*, λ_{u} , are plotted as a function of GdnHCl concentration. When determined

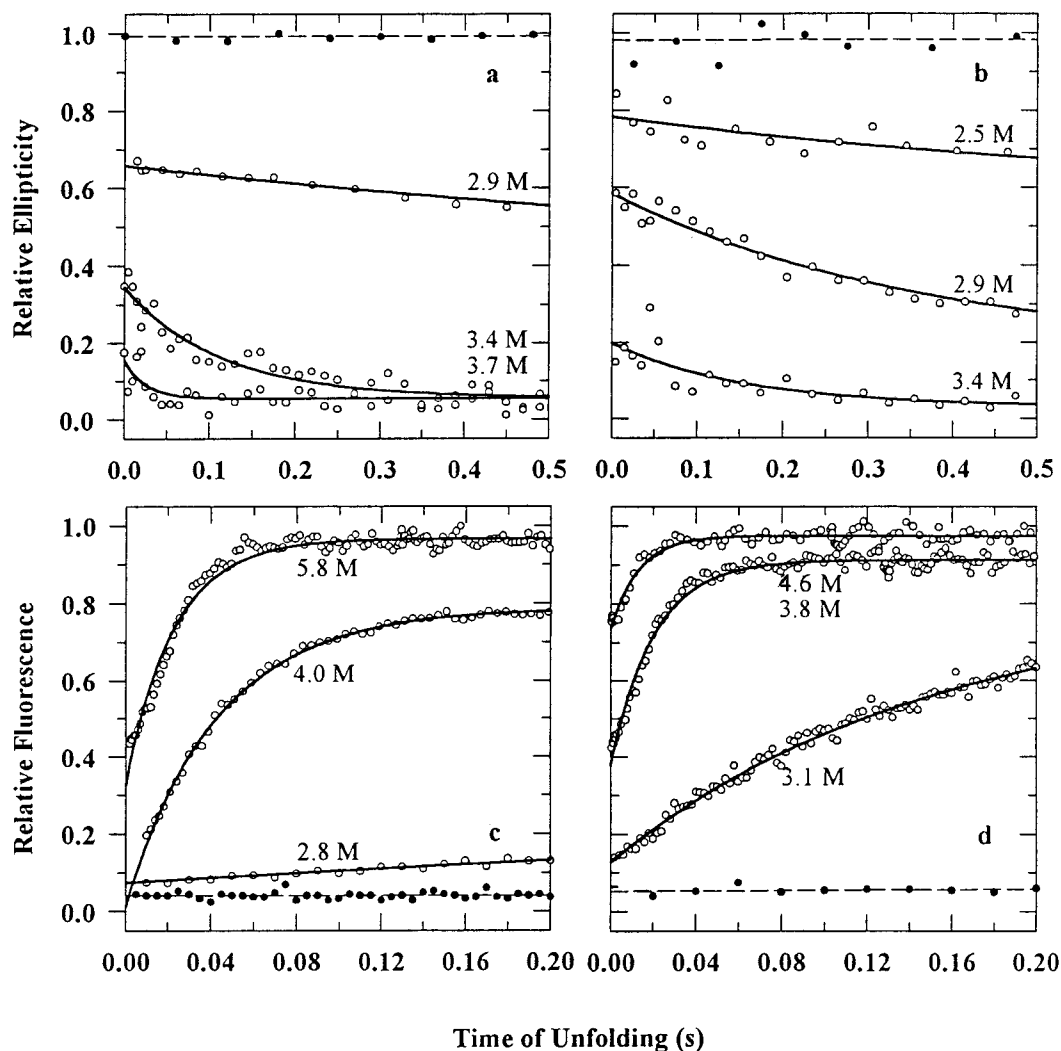


FIGURE 1: Representative stopped-flow kinetic traces of ferricytochrome *c* unfolding in 0.1 M phosphate buffer, pH 7, monitored by far-UV CD at 10 °C (a) and 22 °C (b), and by tryptophan fluorescence at 10 °C (c) and 22 °C (d). The final denaturant concentration in the unfolding medium is indicated for each trace. Each panel also shows the respective signal intensity for the native protein. The solid lines through the data represent nonlinear least-squares best fits of the data to single-exponentials. Kinetic data were recorded for sufficiently long time required to reach equilibrium. For illustration of the initial signal change the traces have been truncated.

from fluorescence-monitored unfolding experiments, $\log \lambda_u$ is seen to increase in a linear manner with an increase in GdnHCl concentration from 2.5 to 4 M. Thereafter, the dependence of $\log \lambda_u$ on GdnHCl concentration, [D], becomes less, leading to a rollover in the plot of $\log \lambda_u$ vs [D]. λ_u appears to have little dependence on denaturant concentrations higher than ~ 4 M GdnHCl. The kinetics of unfolding by GdnHCl concentrations greater than 4 M could not be monitored reliably by far-UV CD because the value of λ_u becomes too large and simultaneously, the observable change becomes too small. In the range of GdnHCl concentrations (2.5–4 M) where the kinetics of unfolding could be determined reliably by both fluorescence and far-UV CD measurements, the two probes yield similar values for λ_u , although the data suggest that the plots of $\log \lambda_u$ vs GdnHCl concentration for the two probes might be diverging at the lowest GdnHCl concentrations.

Unfolding Kinetics at 22 °C. Burst phase changes in not only ellipticity but also fluorescence are seen for unfolding at 22 °C. Figure 3a,b show that at 22 °C, the burst phase decrease in ellipticity as well as the burst phase increase in fluorescence changes cooperatively with GdnHCl concentra-

tion. Both sets of equilibrium unfolding transitions and burst phase unfolding transitions were fit to two-state unfolding transitions, and the values of the thermodynamic parameters are listed in the legend to Figure 3. Analysis of the equilibrium unfolding transitions using eq 1 shows that with respect to the fully unfolded form, U, the fully folded form N becomes marginally destabilized at 22 °C compared with 10 °C. The midpoint of the far-UV CD-monitored burst phase unfolding transition also moves marginally from 3.3 M at 10 °C to 3.1 M GdnHCl at 22 °C, suggesting that the product of the burst phase unfolding transition is also less stable at the higher temperature.

Unfolding becomes faster at 22 °C, as seen in Figure 3c. As at 10 °C, a rollover is seen in the plot of $\log \lambda_u$ vs GdnHCl concentration for the fluorescence-monitored unfolding kinetics at higher (> 3.7 M) concentrations of GdnHCl. Far-UV CD-monitored unfolding was restricted to concentrations of GdnHCl below 3.4 M, because the observable change in ellipticity becomes too small for unfolding by higher concentrations. Far-UV CD- and fluorescence-monitored values for λ_u appear to be identical for measurements of unfolding by GdnHCl between 2.8 and 3.4 M, but are

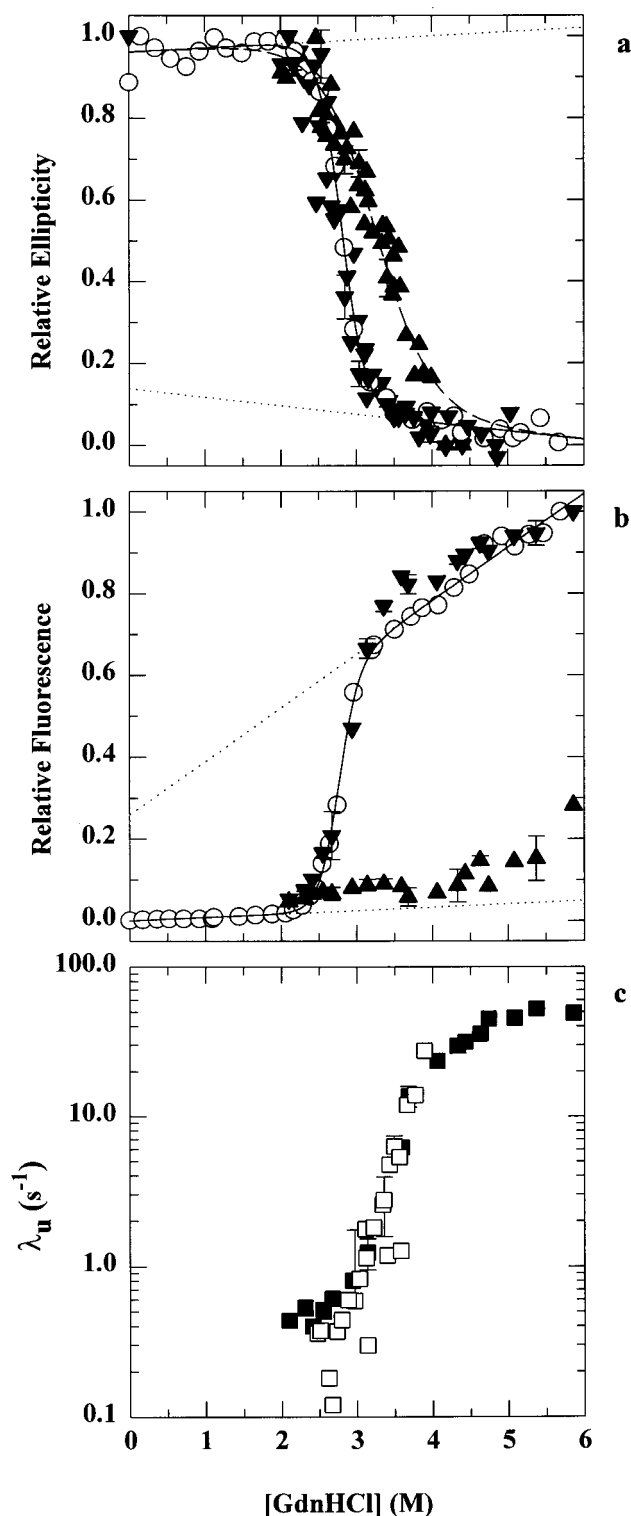


FIGURE 2: Kinetics of unfolding at 10 °C. Panels (a) and (b): Kinetic and equilibrium amplitudes of unfolding were determined by far-UV-CD (a) as well as by fluorescence (b). The initial ($t = 0$) and final ($t = \infty$) values of the spectroscopic signal, A_0 (\blacktriangle) and A_∞ (\blacktriangledown), respectively, obtained from fitting the observable kinetic unfolding curves, are shown relative to the equilibrium unfolding curves (\circ), as described in the text. At a particular GdnHCl concentration, the difference between the A_0 value and the extrapolated native baseline, represented by the dotted line, describes the unobservable (burst phase) amplitude lost in the dead-time (4 ms) of the stopped-flow measurement of the unfolding kinetics. The solid lines in (a) and (b) represent nonlinear least-squares fits of the equilibrium unfolding data to a two-state $F \rightleftharpoons U$ transition (eq 1), and yield values for ΔG_{FU} (kcal mol $^{-1}$) and m_{FU} (kcal mol $^{-1}$ M $^{-1}$)

significantly different for the lowest concentration of GdnHCl (2.4 M) used (Figure 3c).

Unfolding Kinetics at 34 °C. Again, burst phase changes are seen in both fluorescence and ellipticity-monitored unfolding. Figure 4a,b shows that the dependence of the burst phase amplitudes on GdnHCl concentration is as cooperative at 34 °C as it is at 22 °C, for measurements by both optical probes. With respect to the measurements at 22 °C, the midpoints of the GdnHCl dependences of the burst phase amplitudes measured by both probes have shifted to lower GdnHCl concentrations: that of the ellipticity-monitored burst phase changes has shifted from 3.1 to 2.9 M, while that of the fluorescence-monitored burst phase changes has shifted from 4.2 to 3.4 M. The values of the thermodynamic parameters obtained by two-state analysis (eq 1) of both sets of equilibrium and burst phase unfolding transitions in Figure 4a,b are listed in the legend to Figure 4. It should be mentioned that limitations of measurement (see below) at the higher concentrations of GdnHCl did not allow experimental determination of the post-transition baselines of the fluorescence-monitored burst phase unfolding transitions at both 34 and 22 °C. Consequently, the post-transition baselines of the corresponding equilibrium unfolding transitions have been used for analysis. This approximation sets the upper limit on the midpoint of the burst phase unfolding transition, but will not alter significantly its slope.

Unfolding is faster at 34 °C (Figure 4c). Fluorescence-monitored apparent unfolding rate constants greater than ~ 150 s $^{-1}$ could not be recorded confidently because of instrumental limitations, coupled with the fact that the observable amplitude decreases simultaneously with the increase in the rate of unfolding in the presence of higher concentration of GdnHCl. Thus, fluorescence-monitored unfolding kinetics were measured only for concentrations of GdnHCl less than 3.7 M, and although the plot of $\log \lambda_u$ vs $[D]$ is clearly nonlinear, there is no distinct rollover as observed for the two lower temperatures. Ellipticity-monitored unfolding kinetics were limited to GdnHCl concentrations less than 3.0 M, for similar considerations. The ellipticity- and fluorescence-monitored values of λ_u are similar around 3 M GdnHCl but the plots of $\log \lambda_u$ vs $[D]$ appear to diverge as the concentration of GdnHCl used to unfold the protein is reduced (Figure 4c).

The important result in Figures 2–4 is that the burst phase unfolding transitions at any temperature are not coincident, when measured by two different optical probes, far-UV CD and fluorescence. Not only are the midpoints of the burst phase unfolding transitions different when measured by the two probes, but so also are the dependences of the burst phase

of 10.1 and 3.6 in (a) and 11.7 and 4.2 in (b). The dashed line in (a) represents a least-squares fit of the A_0 values also to a two-state $F \rightleftharpoons U$ transition (eq 1), and yields values for ΔG_{FU} (kcal mol $^{-1}$) and m_{FU} (kcal mol $^{-1}$ M $^{-1}$) of 4.9 and 1.5, respectively. The errors in the determination of the values of ΔG and m were approximately $\pm 15\%$. Panel (c): GdnHCl concentration-dependence of the observed rates of unfolding. Apparent rates of unfolding were determined from single-exponential fits to both far-UV CD (\square) and fluorescence (\blacksquare) monitored unfolding kinetics (see Figure 1). Although a few data points show substantially larger errors, the average error in the determination of the apparent rate constants, as determined from 2 or 3 repetitions of each experiment, was less than $\pm 5\%$.

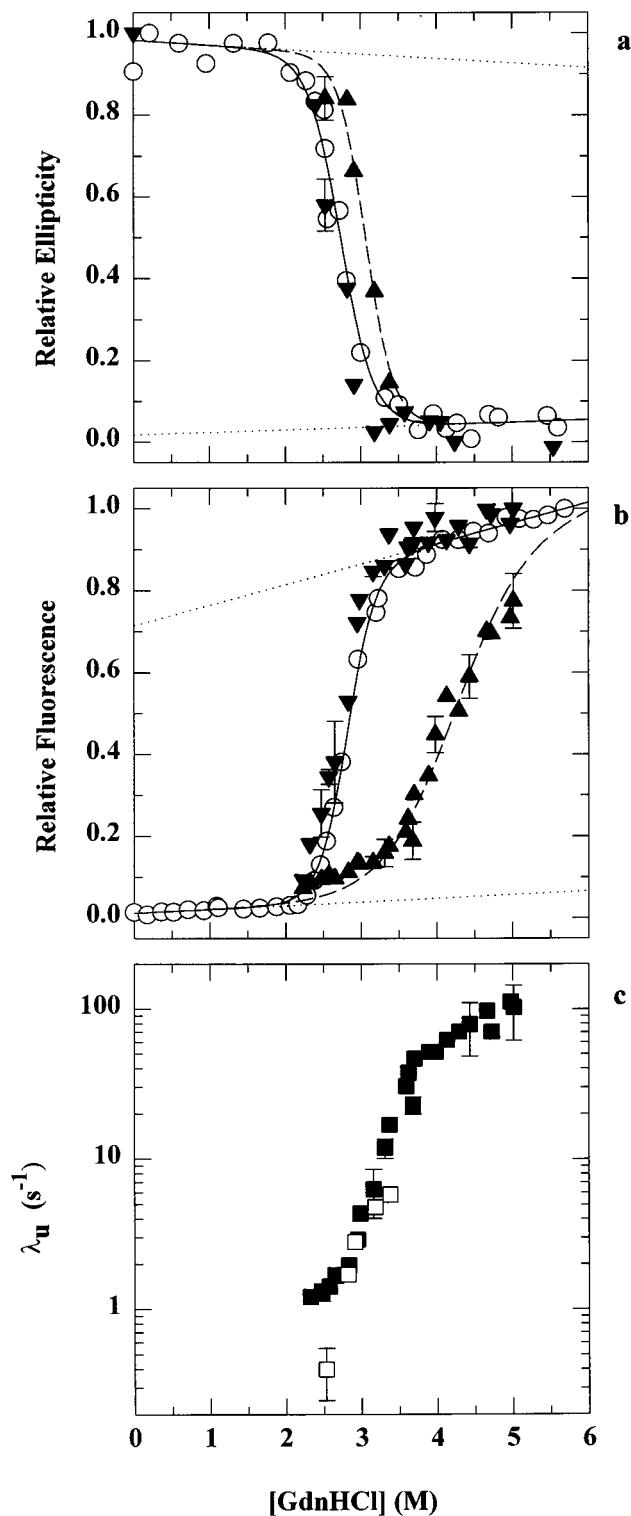


FIGURE 3: Kinetics of unfolding at 22 °C. Panels (a) and (b): Kinetic and equilibrium amplitudes of unfolding were determined by far-UV-CD (a) as well as by fluorescence (b). Symbols and lines are as described in the legend to Figure 2. Nonlinear least-squares fits of the equilibrium unfolding data to a two-state $F \rightleftharpoons U$ transition (eq 1) yield values for ΔG_{FU} (kcal mol⁻¹) and m_{FU} (kcal mol⁻¹ M⁻¹) of 7.7 and 2.8 in (a) and 8.4 and 3.0 in (b). Least-squares fits of the A_0 values to a two state $F \rightleftharpoons I$ transition (eq 1) yield values for ΔG_{FI} (kcal mol⁻¹) and m_{FI} (kcal mol⁻¹ M⁻¹) of 10.1 and 3.3 in (a) and 5.0 and 1.2 in (b). The errors in the determination of the values of ΔG and m were approximately $\pm 15\%$. Panel (c): GdnHCl concentration-dependence of the observed rates of unfolding, as described in Figure 2.

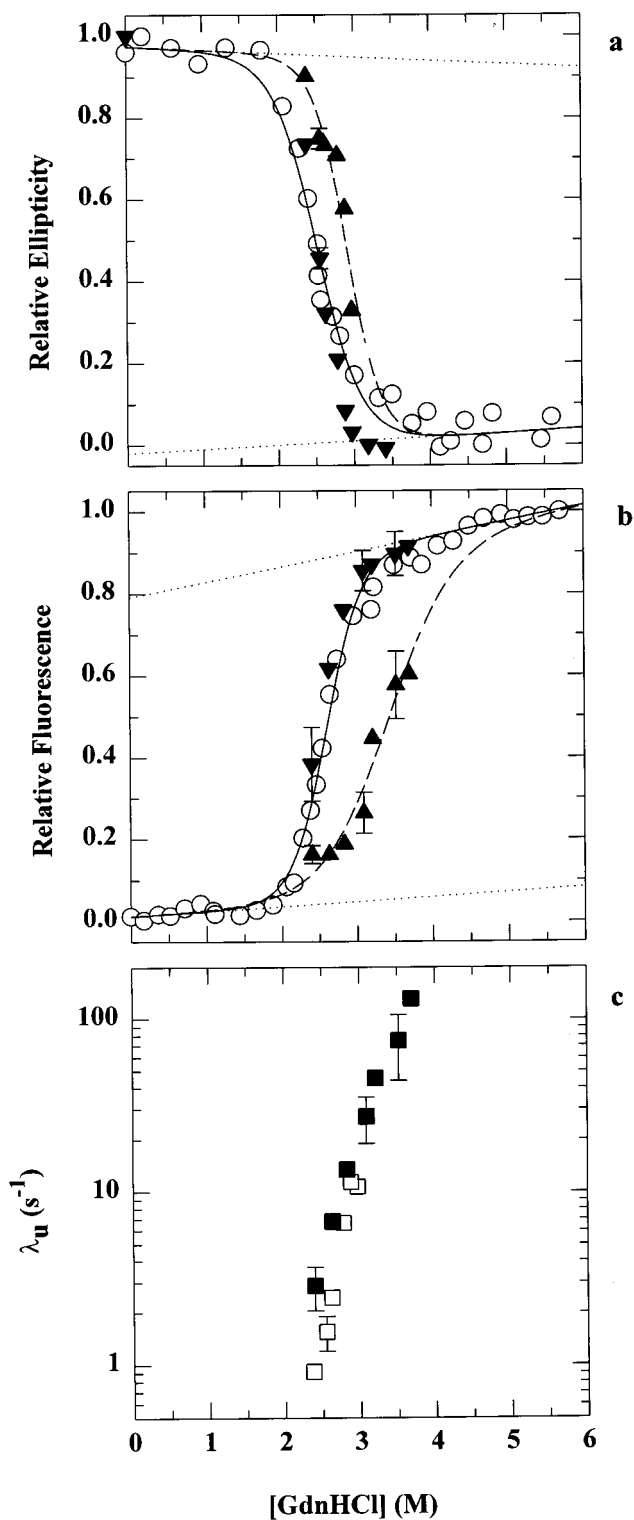


FIGURE 4: Kinetics of unfolding at 34 °C. Panels (a) and (b): Kinetic and equilibrium amplitudes of unfolding were determined by far-UV-CD (a) as well as by fluorescence (b). Symbols and lines are as described in the legend to Figure 2. Nonlinear least-squares fits of the equilibrium unfolding data to a two-state $F \rightleftharpoons U$ transition (eq 1) yield values for ΔG_{FU} (kcal mol⁻¹) and m_{FU} (kcal mol⁻¹ M⁻¹) of 5.2 and 2.1 in (a) and 6.4 and 2.4 in (b). Least-squares fits of the A_0 values also to a two state $F \rightleftharpoons I$ transition (eq 1) yield values for ΔG_{FI} (kcal mol⁻¹) and m_{FI} (kcal mol⁻¹ M⁻¹) of 7.9 and 2.7 in (a) and 4.4 and 1.3 in (b). The errors in the determination of the values of ΔG and m were approximately $\pm 15\%$. Panel (c): GdnHCl concentration-dependence of the observed rates of unfolding, as described in Figure 2.

amplitudes on GdnHCl concentration, as seen in the marked difference in the m values obtained from the two-state fits (see legends to Figures 2–4). It is stressed that the burst phase unfolding transitions in Figures 2–4 have been analyzed according to two-state unfolding transitions only to provide gross estimates for the midpoints of the transitions and the m values, to reinforce the primary observation that the two probes yield noncoincident transitions. Clearly, the noncoincidence of midpoints and slopes of the burst phase unfolding transitions measured by the two probes suggest that at least two kinetic intermediates accumulate during the burst phase of unfolding (see below).

DISCUSSION

Nonlinear Dependence of the Logarithm of Unfolding Rate Constants on Denaturant Concentration. The nonlinear dependence of the logarithm of the apparent unfolding rate constant on GdnHCl concentration for ferricyt *c* was first observed many years ago (6). This original observation has been augmented by recent fluorescence-monitored unfolding studies of ferricyt *c* that have demonstrated distinct rollovers in plots of the logarithm of the apparent unfolding rate constant vs GdnHCl concentration at high concentrations of the denaturant (7–10). Deligation of M80 from the heme, with very little concomitant structural unfolding, has been implicated as the first step during the unfolding of ferricyt *c* (9, 14, 15), and it has been proposed that this might be the rate-limiting step at high concentrations of GdnHCl, causing the denaturant-dependent rate profile to level off in the post-transition region with a near-zero m value (15). In fact, when unfolding at 10 °C is probed via heme absorbance at 695 nm, which is a reliable marker for persistent bonding of M80 to the Fe³⁺ atom (16, 17), the observed rate–denaturant profile is identical with that seen for fluorescence (7, 8, 18). Ascribing the rollover in the denaturant vs unfolding rate profile to deligation of M80 is, however, questionable because the rollover is also seen for unfolding reactions of ferricyt *c* in which M80 coordination to Fe³⁺ is abolished by extrinsically added imidazole (10). Furthermore, at least one limiting process, the rate of which is larger than the rate of deligation of M80 has been probed by the use of heme absorbance at the Soret line (A.K.B., unpublished result).

Thus, what specific structural disruption in ferricyt *c* produces the rollover is open to investigation. Nonlinear plots of logarithm of observed unfolding rate vs GdnHCl concentration has also been seen for several other proteins, including arc repressor (19), α lactalbumin (20), barstar (5), barnase mutants (21), β -lactamase (22), parvalbumin (23), and ribonuclease T2 (24). In the case of the arc repressor, the nonlinear relationship was attributed to the presence of unstable unfolding intermediates, with the rate-limiting step during unfolding changing with denaturant concentration (19), but no direct evidence for the presence of such intermediates was available. Such evidence has only been presented in the case of barstar (5). The available data suggest that the rollover observed for ferricyt *c* is associated with accumulation of kinetic intermediate(s) during unfolding.

Burst-Phase Changes in Optical Signals during the Unfolding of cyt c. The folding and unfolding reactions of cyt *c* have been studied extensively in the microsecond to

seconds time domain using a variety of spectroscopic techniques, but principally absorbance and fluorescence. The existence of submillisecond changes in both fluorescence and far-UV CD during folding are well documented from stopped-flow measurements where they occur in unobservable burst phases (see, for example, ref 8). Jet-mixing continuous flow measurements have also demonstrated the occurrence of a burst phase change in fluorescence, within 50 μ s of commencement of folding (10). Surprisingly, no burst phase change in fluorescence or Soret absorbance during unfolding has been reported previously. The likely reasons could be the following. (a) Most recent studies of the folding and unfolding of ferricyt *c* have been carried out at 10 °C, using fluorescence or Soret absorbance to monitor the reactions. Unlike in the case of folding studies, scarce attention has been paid to quantitation of the amplitudes of spectroscopic changes during unfolding, except in fluorescence-monitored unfolding studies at 10 °C, where no burst phase change was reported to occur, as is also seen in this study (see Figure 2b). (b) Unlike in the case of folding, far-UV CD has not been used to monitor unfolding of cyt *c* at any temperature. As shown here, burst phase changes in far-UV CD are seen for unfolding at all temperatures studied.

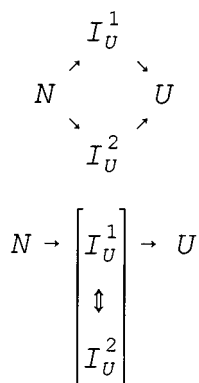
The major conclusion of this study, namely that multiple structurally distinct intermediates accumulate during the unfolding of ferricyt *c* (see below), is dependent critically on the analysis of the amplitudes of the burst phase changes in far-UV CD and fluorescence, the rates of which are too fast to be measured in the millisecond measurements reported here. It was therefore important to be certain that the burst phase changes do not represent experimental artifacts. Important control experiments have been described previously (4). Previous experiments with barstar (5), similar to those reported here with ferricyt *c*, have also shown that changes in environmental conditions or the introduction of a conservative mutation, both of which affect the stability of unfolding intermediates, can lead to enhanced burst phase changes in either fluorescence or far-UV CD or both. In the case of ferricyt *c*, it is seen that reduction of the temperature from 22 to 10 °C leads virtually to a complete absence of a burst phase change in fluorescence but not in far-UV CD (Figures 2 and 3). Moreover, no burst phase changes in far-UV CD or fluorescence are observed for unfolding of cyt *c* in the reduced state at 10 °C (A. K. Bhuyan and J. B. Udgaonkar, unpublished observations). Thus, the burst phase changes observed here must be real and can be attributed to the accumulation of kinetic unfolding intermediates.

It should also be mentioned that in one of the earliest folding studies (25) on ferricyt *c*, in which temperature jumps were used to monitor the unfolding relaxations via Soret absorption, a major, very fast ($\sim 20 \mu$ s) unfolding phase was observed. Rates faster than those reported here have also been observed during GdnHCl-induced unfolding of cyt *c* monitored by heme absorbance at the Soret band (26).

Accumulation of Two Burst Phase Kinetic Intermediates during Unfolding of Oxidized cyt c. The experimental criteria useful to test the presence of unfolding kinetic intermediate(s) are (4, 5): (1) curvature in the plots of logarithm of observed unfolding rates vs denaturant concentration, (2) occurrence of burst phase change of spectroscopic signal amplitude during unfolding, and (3) the noncoincidence of

unfolding kinetics measured by more than one physical probe. As Figures 2–4 show, the first two criteria are fully met for ferricyt *c*. Thus, at least one kinetic intermediate must accumulate in the burst phase during the unfolding of cyt *c*. The noncoincidence of the burst phase unfolding transitions (see Results), when measured by far-UV CD and fluorescence, suggests in fact that at least two kinetic intermediates must accumulate in the burst phase, one (I_U^1) which has lost only native-like ellipticity at 222 nm, and another (I_U^2) which has lost both native-like ellipticity at 222 nm and fluorescence.

Mechanism for Unfolding. Two minimal mechanisms for unfolding, incorporating the intermediates I_U^1 and I_U^2 can be envisaged.



In mechanism 1, I_U^1 and I_U^2 are formed rapidly on two parallel pathways. On each pathway, a rapid preequilibrium is established between N and I_U^1 and/or I_U^2 before either intermediate can unfold to U. In this mechanism, the $N \rightleftharpoons I_U^1$ equilibrium as well as the $N \rightleftharpoons I_U^2$ equilibrium is dependent on temperature and GdnHCl concentration. In mechanism 2, I_U^1 , which forms rapidly from N, preequilibrates rapidly with an ensemble of intermediates that include I_U^2 . The $N \rightleftharpoons I_U^1$ equilibrium and the equilibria between the intermediates comprising the ensemble are all dependent on temperature and GdnHCl concentration.

Since the rates of formation of I_U^1 and I_U^2 are too fast to be measured, the appropriateness of either mechanism for describing the data in Figures 2–4 can only be inferred indirectly from an analysis of the burst phase unfolding transitions determined using the two optical probes. Crucial is the observation that the far-UV CD-monitored and fluorescence-monitored burst phase unfolding transitions are not coincident at any temperature (Figures 2–4). The two probes yield different values for the midpoint of the burst phase unfolding transition (the C_m value) as well as the dependence of the burst phase change in optical signal on GdnHCl concentration (the m value). Thus, while both I_U^1 and I_U^2 are formed in the initial burst phase, the extents to which they accumulate, as represented by the burst phase changes in far-UV CD and fluorescence, are different at any particular GdnHCl concentration; furthermore, the dependences of their extents of accumulation on GdnHCl concentration are different. This observation suggests that mechanism 2 is less appropriate in describing the results.

Consider, for example, the data for unfolding at 22 °C in Figure 3. For unfolding by 2.5 M GdnHCl, more than 95% of the far-UV CD change occurs in the burst phase while

less than 5% of the fluorescence change occurs in the burst phase. Thus, if unfolding were to be occurring via mechanism 2, the ensemble of intermediates formed in the burst phase of unfolding would consist of predominantly I_U^1 for unfolding in 2.5 M GdnHCl. As the concentration of GdnHCl used to unfold the protein is increased, more and more I_U^2 is formed from I_U^1 ; consequently, the ensemble formed in the burst phase will contain a larger proportion of I_U^2 , and a burst phase change in fluorescence will also be observed. Thus according to mechanism 2, the far-UV CD-monitored burst phase unfolding transition in Figure 3 measures essentially only the $N \rightleftharpoons I_U^1$ preequilibrium transition, while the fluorescence-monitored burst phase unfolding transition reports only on the $I_U^1 \rightleftharpoons I_U^2$ preequilibrium transition. Now while the m value of the former transition is similar to the m value of the $N \rightleftharpoons U$ equilibrium unfolding transition, the sum of the m values of the two burst phase unfolding transitions exceeds significantly the m value of the $N \rightleftharpoons U$ equilibrium unfolding transition (see legend to Figure 3). Since the m value of an unfolding transition represents the additional nonpolar surface area exposed upon unfolding, this would imply that I_U^2 has more nonpolar surface area exposed than U. Clearly this is very unlikely, because U represents completely unfolded protein. Such an indirect analysis therefore suggests that mechanism 2 is not appropriate to describe the data in Figure 3. In contrast, if I_U^1 and I_U^2 are formed in parallel pathways as in mechanism 1 and not sequentially as in mechanism 2, the m values of the two burst phase unfolding transitions in Figure 3 represent different degrees of nonpolar solvent exposure that occur in two competing initial steps of unfolding, and the only requirement is that each m value be less than or equal to the m value of the equilibrium $N \rightleftharpoons U$ unfolding transition. This requirement is met, and mechanism 1 would therefore appear appropriate to describe unfolding. Nevertheless, it must be emphasized that direct resolution of the rates of formation of I_U^1 and I_U^2 , in addition to the rates of their unfolding, will be necessary to show conclusively the appropriateness of the use of mechanism 1 to describe the unfolding of ferricyt *c*.

Mechanism 1 has also been used to describe the unfolding of barstar (5). In that case, the proposal for the existence of two parallel pathways received additional support from observations not evident in the present study with ferricyt *c*. It was found that (1) fluorescence and far-UV CD-monitored unfolding rates were different, (2) the dependences of these rates on denaturant concentration were different, and (3) it was possible to define different unfolding conditions where only a burst change in fluorescence could be observed, unfolding conditions where only a burst phase change in far-UV CD could be observed, and unfolding conditions where burst phase changes in both fluorescence and far-UV CD could be observed.

Folding and Unfolding Pathways. The landscape description of protein folding and unfolding (27–29) poses an important question mentioned in the introductory section: is the folding reaction an exact reversal of the unfolding process, given that folding and unfolding reactions are carried out under vastly different conditions? It need not be because (a) on a multidimensional energy surface the trajectories of protein motions during folding may not be the same for unfolding, and (b) the conformational space spanned by the

unfolded polypeptide is larger than that for the native protein. On the other hand, a consideration of experimental results for folding and unfolding of some proteins (5) shows that protein folding and unfolding reactions appear to follow the same pathway (30), but the rate-limiting step changes with a change from folding to unfolding conditions (19). In the case of barstar, Zaidi et al. (5) find a reciprocal relationship of structure formation and dissolution during folding and unfolding. During folding of barstar via the major pathway, a nonspecific hydrophobic collapse yielding a compact form of the protein is followed by secondary structure formation. The sequence of events is reversed during unfolding via one of the two unfolding pathways detected for this protein. The other unfolding pathway appears to have the reciprocal relationship with the minor folding pathway.

In the case of ferricyt *c*, an early folding intermediate containing a large fraction of secondary structure but lacking any significant amount of tertiary interactions has been described (14, 30, 31). The results presented here indicate that during unfolding by 2.5 M GdnHCl at 22 °C (Figure 3), secondary structure is lost before the loss of certain tertiary contacts, suggesting an apparent reversal of events. It may be noted that the early intermediate during the folding of ferricyt *c* is known to be a misfolded species (32). The protein folds in an apparent two-state manner when the iron-histidine bond in the unfolded state is eliminated by lowering the pH of the folding medium (8) or by adding a suitable ferric iron ligand in the unfolded protein solution (10).

Structural Properties of the Unfolding Intermediates. I_U^1 possesses a mean residue ellipticity at 222 nm corresponding to that of the unfolded protein, U, while the mean residue ellipticity at 222 nm as well as the fluorescence of I_U^2 appears to be similar to that of U. How are these intermediates, in particular I_U^2 , structurally different from U? It is clear from the data in Figures 2–4 that the stabilities of the kinetic intermediates, as represented by the midpoints of the burst phase unfolding transitions, decrease with an increase in temperature from 10 to 34 °C. It has been suggested that hydrophobic interactions stabilizing protein structures are strongest at 22 ± 5 °C (33), and they are expected to be weaker at both the lower (10 °C) and higher temperatures (34 °C) used in this study. The decrease in stability of the intermediates with an increase in temperature from 10 to 22 °C suggests that, in addition to hydrophobic interactions, hydrogen bonding interactions are also important in defining the stabilities of the unfolding intermediates. Since hydrogen-bonded secondary structure is not present in the unfolding intermediates, it is not obvious what other type of hydrogen-bonded structure might be present in the intermediates.

The nature of the structural element that might be present in the unfolding intermediates can only be speculated upon at the present time. To do so, it is useful to look at the results of native-state hydrogen exchange studies of ferricyt *c* (30), which allow the detection of partially unfolded forms that can exist in equilibrium with the fully folded protein. One such partially unfolded form that has been identified is the segment of residues 36 to 61, which forms a large omega loop (34) that encloses a network of hydrogen bonds in the environment of W59 and the heme (35), which is referred to as the HP-7 hydrogen bonding network. Thus, one possibility for a hydrogen-bonded network not involving a secondary structural element, which might be present in the

intermediates is the HP-7 hydrogen bonding network. Pulse-labeling hydrogen exchange studies are being used to determine whether the conjecture that the HP-7 network is retained in the unfolding intermediates, is indeed correct. It appears that evolution has conserved a similar but nonexact hydrogen bonding network in the class I *c*-type cytochromes (35–38; see also refs 39, 40).

Multiple Kinetic Intermediates in Protein Unfolding. In this study, it has been shown that at least two structurally distinct kinetic intermediates accumulate during the unfolding of ferricyt *c*. These intermediates equilibrate rapidly with the fully folded state before the start of the observable unfolding reaction. It has been assumed in this study that both kinetic unfolding intermediates are productive, leading directly to production of the globally unfolded state, but the possibility that they are kinetic dead-ends and therefore nonproductive intermediates cannot be ruled out.

It has been suggested here that the two burst phase kinetic intermediates accumulate on two competing pathways that are available for cyt *c* to unfold by. This inference of the data reported here needs to be confirmed by unfolding studies that utilize the elegant microsecond mixing methods that have only recently been applied to the study of ferricyt *c* folding (41–43). If two pathways are indeed present, the properties of the transition state governing each of the two pathways can be inferred from the properties of the intermediate immediately preceding the rate-limiting step on that pathway, and the two transition states on the two parallel pathways would therefore be expected to be very dissimilar structurally. The observation that the two optical probes yield similar rates for the rate-limiting steps in unfolding suggests that the transition states represent similar energy barriers to unfolding. It should, however, be noted that the formal possibility that the two intermediates converge to a common transition state cannot be ruled out. The results reported here lend support to the energy landscape view of protein folding and unfolding (28, 29, 43) in which multiple pathways are available for protein folding or unfolding.

ACKNOWLEDGMENT

We thank R. L. Baldwin and U. Nath for their comments on the manuscript.

REFERENCES

1. Kiefhaber, T., Labhardt, A. M., and Baldwin, R. L. (1995) *Nature* 375, 513–515.
2. Phillips, C. M., Mizutani, Y., and Hochstrasser, R. M. (1995) *Proc. Natl. Acad. Sci. U.S.A.* 92, 7292–7296.
3. Hoeltzli, S. D., and Frieden, C. (1995) *Proc. Natl. Acad. Sci. U.S.A.* 92, 9318–9322.
4. Nath, U., Agashe, V. R., and Udgaonkar, J. B. (1996) *Nat. Struct. Biol.* 3, 920–923.
5. Zaidi, F. N., Nath, U., and Udgaonkar, J. B. (1997) *Nat. Struct. Biol.* 4, 1016–1024.
6. Ikai, A., Fish, W. W., and Tanford, C. (1973) *J. Mol. Biol.* 73, 165–184.
7. Bhuyan, A. K. (1995) Ph.D. Thesis, University of Pennsylvania, Philadelphia, PA.
8. Sosnick, T. R., Mayne, L., and Englander, S. W. (1996) *Proteins* 24, 413–426.
9. Colón, W., Elöve, G. A., Wakem, L. P., Sherman, F., and Roder, H. (1996) *Biochemistry* 35, 5538–5549.
10. Chan, C.-K., Hu, Y., Takahashi, S., Rousseau, D. L., Eaton, W. A., and Hofrichter, J. (1997) *Proc. Natl. Acad. Sci. U.S.A.* 94, 1779–1784.
11. Pace, C. N. (1986) *Methods Enzymol.* 131, 266–280.

12. Santoro, M. M., and Bolen, D. W. (1988) *Biochemistry* 27, 8063–8068.
13. Agashe, V. R., and Udgaonkar, J. B. (1995) *Biochemistry* 34, 3286–3299.
14. Elöve, G. A., Bhuyan, A. K., and Roder, H. (1994) *Biochemistry* 33, 6925–6935.
15. Sauder, J. M., MacKenzie, N. E., and Roder, H. (1996) *Biochemistry* 35, 16852–16862.
16. Schechter, E., and Saludjian, P. (1967) *Biopolymers* 5, 788–790.
17. Kaminsky, L., Miller, V. J., and Davison, A. J. (1973) *Biochemistry* 12, 2215–2220.
18. Ridge, J. A., Baldwin, R. L., and Labhardt, A. M. (1981) *Biochemistry* 20, 1622–1630.
19. Jonsson, T., Waldburger, C. D., and Sauer, R. T. (1996) *Biochemistry* 35, 4795–4802.
20. Ikeguchi, M., Kuwajima, K., Mittani, M., and Sugai, S. (1986) *Biochemistry* 25, 6965–6972.
21. Matoushcek, A., Matthes, J. M., Johnson, C. M., and Fersht, A. R. (1994) *Protein Eng.* 7, 1089–1095.
22. Vanhove, M., Raquet, X., and Frere, J.-M. (1995) *Proteins: Struct., Funct., Genet.* 22, 110–118.
23. Lin, L.-N., and Brandts, J. F. (1978) *Biochemistry* 17, 4102–4110.
24. Kawata, Y., and Hamaguchi, K. (1995) *Protein Sci.* 4, 416–420.
25. Tsong, T. Y. (1973) *Biochemistry* 12, 2209–2214.
26. Tsong, T. Y. (1976) *Biochemistry* 15, 5467–5473.
27. Wolynes, P. G., Onuchic, J. N., and Thirumalai, D. (1995) *Science* 267, 5204–5205.
28. Dill, K. A., and Chan, H. S. (1997) *Nat. Struct. Biol.* 4, 1–19.
29. Chan, H. S., and Dill, K. A. (1998) *Proteins: Struct., Funct., Genet.* 30, 2–33.
30. Bai, Y., Sosnick, T. R., Mayne, L., and Englander, S. W. (1995) *Science* 269, 192–197.
31. Roder, H., Elöve, G. A., and Englander, S. W. (1988) *Nature* 335, 700–704.
32. Sosnick, T. R., Mayne, L., Hiller, R., and Englander, S. W. (1994) *Nature Struct. Biol.* 1, 149–156.
33. Baldwin, R. L. (1986) *Proc. Natl. Acad. Sci. U.S.A.* 83, 8069–8072.
34. Leszczynski, J. F., and Rose, G. D. (1986) *Science* 234, 849.
35. Bushnell, G., Louie, G., and Brayer, G. (1990) *J. Mol. Biol.* 214, 585–595.
36. Oichi, H., Hata, Y., Tanaka, N., Kakudo, M., Sakurai, T., Aihara, S., and Morita, Y. (1983) *J. Mol. Biol.* 166, 407–418.
37. Louie, G., and Brayer, G. (1990) *J. Mol. Biol.* 214, 527–555.
38. Caffrey, M. S., Daldal, F., Holden, H. M., and Cusanovich, M. A. (1991) *Biochemistry* 30, 4119–4125.
39. Takano, T., and Dickerson, R. E. (1980) *Proc. Natl. Acad. Sci. U.S.A.* 77, 6371–6375.
40. Takano, T., and Dickerson, R. E. (1981) *J. Mol. Biol.* 153, 95–115.
41. Takahashi, S., Yeh, S.-R., Das, T., Chan, C.-K., Gottfried, D. S., and Rousseau, D. L. (1997) *Nat. Struct. Biol.* 4, 44–50.
42. Chan, C.-K., Hu, Y., Takahashi, S., Rousseau, D. L., Eaton, W. A., and Hofrichter, J. (1997) *Proc. Natl. Acad. Sci. U.S.A.* 94, 1779–1784.
43. Lazaridis, T., and Karplus, M. (1997) *Science* 278, 1928–1931.

BI980470U